ELSEVIER

Journal of Organometallic Chemistry 568 (1998) 1–12

Journal of Organometallic Chemistry

Organolead(IV) polymers $[(Me_3Pb)_4M(CN)_6 \cdot nH_2O]$ with M = Fe and Ru ($0 \leq n \leq 2$): solid-state NMR and vibrational spectroscopy; crystal structure of the dihydrates

Abdul K. Brimah [a,b], Peter Schwarz [b], R.D. Fischer [b,*], Nicola A. Davies [c], Robin K. Harris [c]

[a] *Department of Chemistry, University of Ghana, Legon, Ghana*
[b] *Institut für Anorganische und Angewandte Chemie der Universität Hamburg, Martin-Luther-King-Platz 6, D-20146 Hamburg, Germany*
[c] *University of Durham, Department of Chemistry, South Road, Durham DH1 3LE, UK*

Received 21 February 1997

Abstract

From aqueous solutions of Me_3PbCl and $K_4[M(CN)_6]$ (4:1; M = Fe or Ru), primarily the diaqua compounds $[(Me_3Pb)_4M(CN)_6 \cdot 2H_2O]$, **4a** and **4b**, precipitate. These turn out to be not the three-dimensional host-guest systems $[\{Me_3Pb(H_2O)_2\}(Me_3Pb)_3M(CN_6)]$, but to consist of infinite, puckered layers whose in-built $-M-C\equiv N-Pb-OH_2$ units are likely to form hydrogen bridges between the layers. **4a** appears to be sensitive to even very modest influences (including grinding) and tends to lose the coordinated H_2O molecules partially or totally. This feature is monitored best by both infrared/Raman and CP MAS solid-state NMR spectroscopy. The strictly anhydrous species, **5a** and **5b**, strongly resemble their earlier-reported Me_3Sn-homologues in also displaying strongly temperature-dependent ^{13}C solid-state NMR spectra, but show no ion-exchange activity. The ^{13}C-, ^{15}N- and ^{207}Pb-NMR data in combination yield detailed information about crystallographic sites and intramolecular mobility ol' the Me_3Pb groups.

Keywords: Lead; Iron; Ruthenium; Cyanide; Polymer; Solid-state NMR; Crystal structure; Magic-angle spinning

1. Introduction

In a recent paper we have described novel organotin(IV) polymers of the type: $[(Me_3Sn)_4M(CN)_6]$ (M = Fe, Ru, Os; **1a**/**b**/**c**) which precipitate spontaneously from aqueous solution when (solvated) Me_3Sn^+- and $[M(CN)_6]^{4-}$-ions are brought together in appropriate concentrations [1]. Although single crystals, of the strictly anhydrous compounds, could not be obtained so far, the asymmetric unit of the three isostructural polymers as well as the local symmetries of their Me_3Sn- and $M(CN)_6$-building blocks have been unambiguously deduced from detailed CPMAS solid-state NMR and infrared/Raman (IR/Ra) spectroscopic results [1]. Apart from the still pending question of the proper supramolecular architecture of **1a**/**b**/**c**, these compounds are of interest in view of their readiness to undergo facile exchange of just one Me_3Sn^+ ion (per formula unit) by a large variety of inorganic, organic and organometallic guest cations, G^{n+} [2–4]:

$$\underset{\text{(insoluble)}}{[(Me_3Sn)_4M(CN)_6]} \overset{1/n\, G^{n+}}{\underset{(H_2O)}{\rightarrow}} \underset{\text{(insoluble)}}{[(G^{n+})_{1/n}(Me_3Sn)_3M(CN)_6]} + \underset{\text{(soluble)}}{[Me_3Sn \cdot aq]^+} \quad (1)$$

Although this reaction resembles a nonreversible ion-exchange process involving a permanently insoluble exchange resin, there is increasing evidence for the assumption that in the above reaction H_2O molecules catalyse a rapidly fluctuating, reversible cleavage of the otherwise infinite $\dashv M-C\equiv N-Sn-N\equiv C\vdash$ chains building up the three-dimensional (3D) host-framework [5]. Almost simultaneously with our investigation of the organotin polymers we have observed that apparently

* Corresponding author. Fax: +49 4041 232893.

0022-328X/98/$19.00
PII S0022-328X(97)00202-7

well-defined, white organolead polymers precipitate whenever sufficiently concentrated aqueous solutions of Me_3PbCl and $K_4[M(CN)_6]$ are united:

$$4Me_3PbCl + K_4[M(CN)_6] \xrightarrow{H_2O} [(Me_3Pb)_4M(CN)_6 \cdot nH_2O] \quad (2)$$

In the following, we report the chemical and spectroscopic properties (solid-state NMR and vibrational spectroscopy) of the resulting products for $0 \leq n \leq 2$, as well as the crystal structures of the dihydrates with M = Fe (**4a**) and Ru (**4b**). One aim of this work has been to arrive, via additional knowledge on the new organolead systems, at a better understanding both of the unprecedented 'ion-exchange' capability and of the architecture of the unsatisfactorily crystallizing anhydrous organotin homologues.

2. Preparation and chemistry of $[(Me_3Pb)_4M(CN)_6 \cdot nH_2O]$-systems

Employment of the analogue of the standard route to prepare **1a**–**1c** [1], i.e. co-precipitation from almost saturated solutions of hydrated Me_3Pb^+- and $[M(CN)_6]^{4-}$-ions followed by extended drying of the precipitates in vacuo at room temperature, did not afford strict homologues of the anhydrous organotin polymers.

Instead, the elemental analyses of the organolead precipitate with M = Fe (**2a**) are reasonably consistent with the formation of a monohydrate. Also, the ν(CN) vibrational spectra of **2a** differ significantly from those of **1a**–**1c** (vide infra). Drying at ca. 80°C, but at ambient pressure (for 1–2 days), has led to products (M = Fe, **3a**; Ru, **3b**) definitely poorer in H_2O whose ν(CN) spectra are still reminiscent of that of **2a**. On the other hand, more modest drying (at room temperature and ambient pressure) of the crystalline product resulting in good yields within a few days from less concentrated, initially clear $Me_3PbCl/K_4[M(CN)_6]$-solutions (4:1) affords the crystalline products **4a** (M = Fe) and **4b** (M = Ru), which could be identified both by elemental analyses and X-ray crystallography (vide infra) as the dihydrates, $[(Me_3Pb)_4M(CN)_6 \cdot 2H_2O]_n$. Only prolonged drying in vacuo at elevated temperatures (60–80°C) leads to the completely anhydrous homologues of **1a** and **1b**, **5a** (Fe) and **5b** (Ru). Both **4a**/**4b** and **5a**/**5b** display simpler ν(CN) spectra than **2a** and **3a**/**b** and are in fact reminiscent of those of the organotin systems **1a**-**1c**. Concomitantly, according to a combined TG/DTA study of **2a**, about one mole of H_2O (per formula unit) is actually lost in the temperature range: 80–90°C.

Thermal decomposition of all organolead polymers takes place at considerably lower temperatures than for the organotin systems (i.e. above ca. 200°C), the colour changing from white to brown. Both families of polymers are practically insoluble in most organic solvents (exceptions: e.g. DMF and DMSO) and H_2O (at pH-values ≤ 7), but none of the new organolead compounds displays the so far unique ion-exchange capability of **1a**-**1c**. For instance, suspensions of either **5a** or **2a** in aqueous solutions of $(Et_4N)Cl$ or $[(C_5H_5)_2Co]ClO_4$ did not, even after prolonged stirring, lead to the likewise insoluble host-guest systems $[(G^+)(Me_3Pb)_3Fe(CN)_6]$ with $G^+ = Et_4N^+$ or $[(C_5H_5)_2Co]^+$. The latter compounds could, however, be prepared by reaction of $[(Me_3Pb)_3Fe^{III}(CN)_6]$ (**6**) [6] with either $(Et_4N)I$ or $[(C_5H_5)_2Co]$ in acetonitrile [7,8]. While the organolead systems do not exchange Me_3Pb^+ for Me_3Sn^+ ions either, various anhydrous, probably 'alloyed', polymers of the type $[(Me_3Sn)_{4-x}(Me_3Pb)_xFe(CN)_6]$ with $0 < x \leq 2$ can be prepared by suspending **1a** in aqueous solutions of Me_3PbCl. The respective Me_3Pb/Me_3Sn ratio was easily determined by quantitative assessment of the ^{1}H-NMR spectra of the completely dissolved polymers (in sufficiently alkaline D_2O/NaOD).

2.1. Vibrational spectra (ν-CN- and ν-PbC-ranges only)

As for **1a**/**b**/**c** [1], the most informative spectral ranges of all $[(Me_3Pb)_4M(CN)_6 \cdot nH_2O]$ species are those of their ν(CN) and ν(PbC) vibrations. The most significant changes taking place in the ν(CN) range when n is varied between 0 and 2.0 are depicted in Figs. 1 and 2. Interestingly, the dihydrate, **4b** (M = Ru), displays just three IR- and three Ra-active ν(CN) bands (Table 1) that seem to avoid IR/Ra-coincidence, suggesting distorted-octahedral, but still centrosymmetric, $Ru(CN)_6$ units of the most probable local point symmetry D_{2h} (vide infra). The IR spectra of various samples of the Fe-homologue, **4b**, gave rise to at least one extra band reflecting some notable sensitivity to the usual techniques of preparing IR-probes. The corresponding Raman spectra of microcrystalline **4a** and **4b** not subjected to any grinding turned out to resemble those of **1a**/**b**/**c**. Samples with n intermediate between 2.0 and 0 display IR- and Ra-spectra with more than three ν(CN) bands, while the two strictly anhydrous species **5a** and **5b** again give rise to three IR- and Ra-active bands only. Although the IR bands turn out to be somewhat broader than for $n = 2$, IR/Ra-coincidence appears to be again circumvented. Interestingly, two (of the three) Ra bands of the dihydrates and of the corresponding anhydrous systems have practically identical wavenumbers.

While the IR-active ν(PbC) absorptions are frequently difficult to detect, the corresponding Ra-spectra of all samples display clearly just one quite intense $\nu(PbC)_{sym}$ and one considerably weaker $\nu(PbC)_{asym}$ band (Table 2). All Ra-spectra look very reminiscent of that of **1c** (Fig. 5 in Ref. 1) and are consistent with the

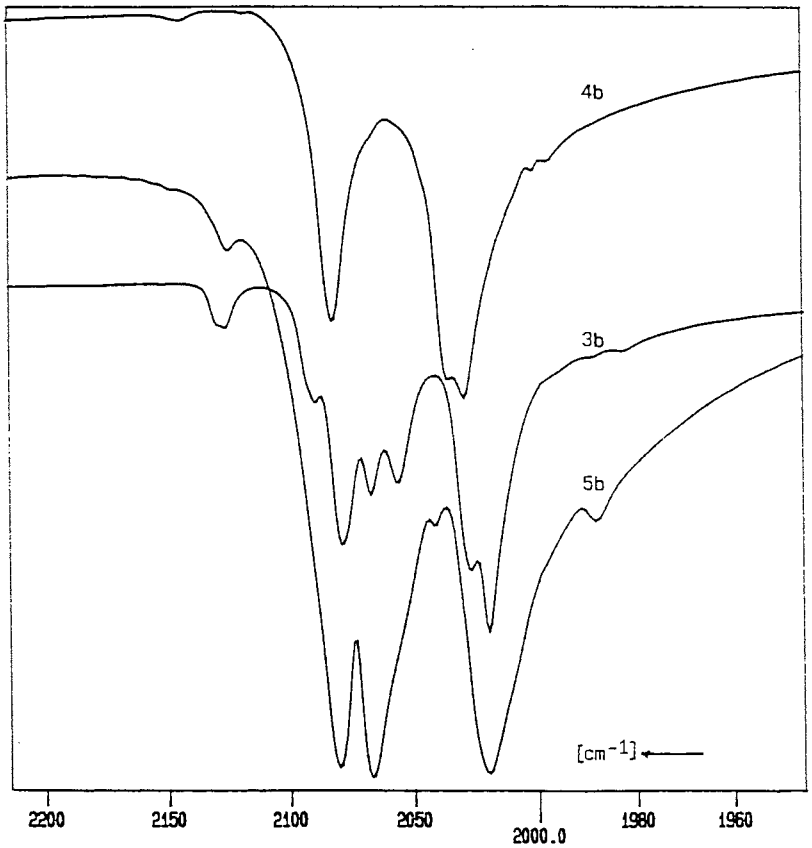

Fig. 1. Infrared spectra in the ν(CN) absorption range of the three related samples **3b**, **4b** and **5b**.

assumption of planar Me_3Pb units. For $n \neq 2$ and 0, only the less intense ν(PbC)-band undergoes occasional splitting. The presence of H_2O (e.g. for **4a** and **4b** embedded in Nujol mulls) is indicated only faintly by a broad band at 1620 cm^{-1}, which becomes notably weaker after exhaustive drying.

2.2. Crystal structures of $[(Me_3Pb)_4M(CN)_6 \cdot 2H_2O]$ ($M = Fe$, **4a**, $M = Ru$, **4b**)

Only slowly-grown, well-shaped crystals of **4a** and **4b** with still partially wet surfaces could be successfully subjected to crystallographic X-ray studies. Crystal data and details of data collection and refinement are given in Table 3. The two homologues are isostructural polymers whose architecture is based upon the cross-linking (at M) of two chains, A (nonlinear, infinite) and B (approximately linear, finite):

A: $\dashv$M–C(1)–N(1)–Pb(1)–N(3)–C(3)–M′–C(3′)
–N(3′)–Pb(1′)–N(1′)–C(1′)$\vdash_\infty$

B: {H(1) H(2)} O(1)–Pb(2)–N(2)–C(2)–M–C(2′)
–N(2′)–Pb(2′)–O(1′) {H(2′) H(1′)}

Pb(1) and Pb(2) as well as C(1)N(1), C(2)N(2) and C(3)N(3) are of equal abundance (see also Fig. 4).

Relevant bond distances and angles are collected in Tables 4 and 5, respectively. The $M(CN)_6$ building blocks are not strictly octahedral, but are centrosymmetric (most probable local point symmetry: D_{2h}; vide supra) and resemble the likewise distorted $Fe(CN)_6$ units of the 3D-polymers $[(Me_3Sn)_4Fe(CN)_6 \cdot 2H_2O \cdot 2L]$ (2L = dioxane, **7** [9] and L = H_2O, **8** [10]) in that one pair of *trans*-oriented CN-ligands carries $Me_3E \cdot OH_2$ groups (E = Pb or Sn). The methyl carbon atoms of the $Me_3Pb(OH_2)$ unit of **4a** turn out to be disordered in that for these C-atoms there are two alternative sets of coordinates (i.e. C(7)–C(9) and C(7′)–C(9′); see Table 9). The N(2)–Pb(2)-distances in chain B of **4a**/**b** are significantly shorter than the distances N(1)–Pb(1) and N(3)–Pb(1) in chain A. As the average C(Me)–Pb(2)–N(2) angle (C(7), C(8) and C(9)) clearly exceeds 90°, the ((CN)$Me_3Pb(OH_2)$) unit may be considered as distorted trigonal bipyramidal (t.b.p.) configured whereas the {(CN)$Me_3Pb(NC)$} unit of chain A is of almost ideal t.b.p. form. The Pb–N distances in chain A (of both homologues) compare well with the Pb–N distances reported for the 3D-polymer $[(Me_3Pb)_3Co(CN)_6]$ (**6**) [6]. The Pb–O distances in **4a** and **4b** significantly exceed even the longer of the two Pb–O distances reported for 1D-polymeric $[Me_3PbOCOCH_3]$ (2.33 and 2.56 Å) [11]. This feature is in accordance with the observation that

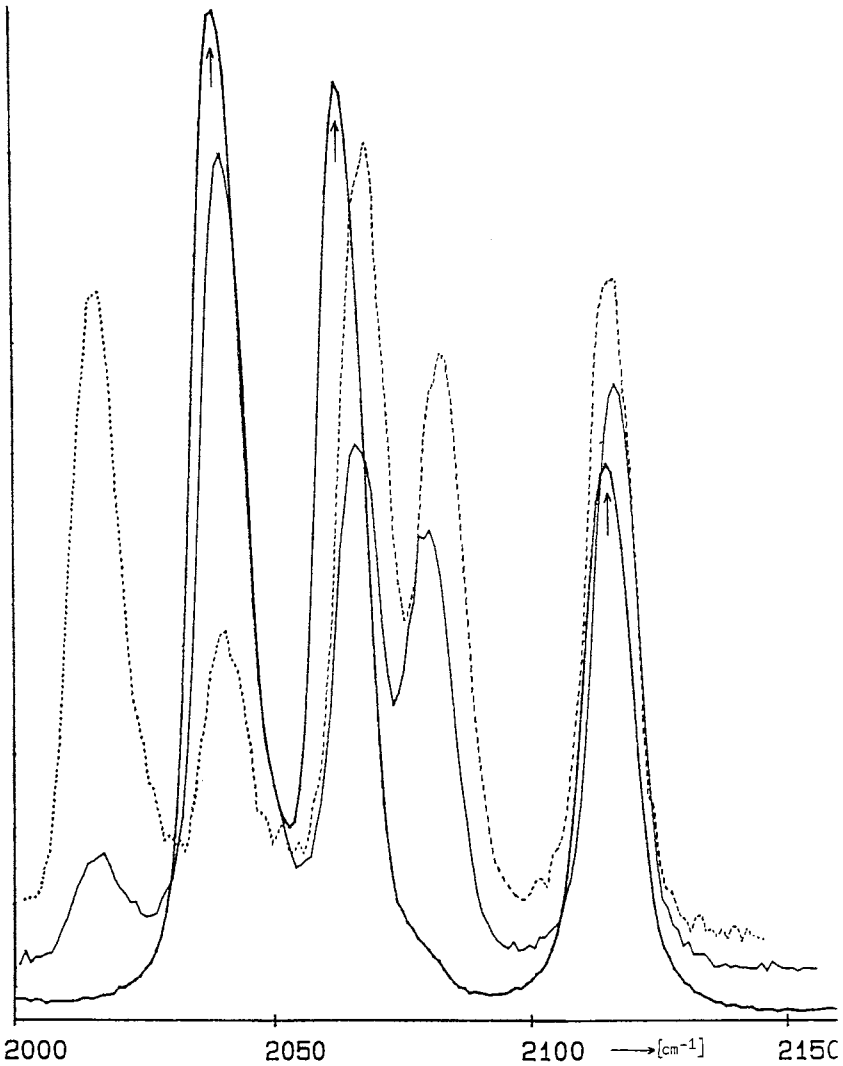

Fig. 2. Raman spectra in the ν(CN) range of **2a**, **3a** (dotted line) and **4a** (bands marked by an arrow). The spectrum of **5a**, which would overlap significantly with that of **4a** is not shown.

both compounds start losing H_2O at very moderate temperature/pressure conditions (vide supra).

All C–N–Pb angles in chain A deviate strongly from 180°, the actual values matching that of the most acute C–N–Pb angle of **6** (125°). As a result of this, significant C–N–Pb bending, chain A gives rise to comparatively compact, puckered layers of infinite extension in the *yz*-plane (Fig. 3). All chains of type B extend approximately perpendicular to these layers, approaching with their terminal OH_2 ligands quite closely to distinct nitrogen atoms of adjacent layers. Actually, all inter-layer O(1)···N(1′) and O(1)···N(3′) distances of **4a** and **4b** (Table 4) would be compatible with the assumption of genuine O – H···N hydrogen bonds. Thus, in principle the nitrogen atoms of all type A chains could be involved in hydrogen bridges so that the primarily layered structures of **4a**/**b** might possibly be considered as true 3D-networks. Similar O – H···N(Sn--)C bridges have been deduced earlier from the crystal structures of **7** and **8** [9,10].

Another feature of interest is that the crystallographic 'formula weight volumes', $V_{fw} = M_r/D_{calc.} = 0.602\ V/Z$ (for the explanation of these symbols see Table 3) of **4a** and **4b** (i.e. 490 and 502 $cm^3\ mol^{-1}$, respectively) lie between the reported [6] values for $[(Me_3Sn)_3Co(CN)_6]$ and $[\{(C_5H_5)_2Co\}(Me_3Sn)_3Fe(CN)_6]$ (460 and 550 $cm^3\ mol^{-1}$, respectively). The packing of **4a** and **4b** may thus be considered as comparatively compact. One might speculate further that (a) the imaginable, isometric host–guest systems: $[\{Me_3Pb(H_2O)_2\}(Me_3Pb)_3M(CN)_6]$ are not likely to reach any more favourable packing conditions, and that (b) the strictly anhydrous species **5a** and **5b** are expected to display even smaller V_{fw}-values than their still dihydrated 'parent' systems.

Table 1
ν(CN) absorptions of various $[(Me_3Pb)_4M(CN)_6 \cdot nH_2O]$ systems from the infrared and Raman spectra (Raman data are underlined)

Sample	ν(CN) in cm^{-1}						
4a		2022 s	2031 sh	2059 w-m		2074 s	
				2039 s	2064 s		2116 s
4b		2030 s	2035 sh			2084 s	
				2050 s		2076 s	2130 ms
2a	2012 s	2023 sh	2031 sh	2059 s		2071 s	2114 w
	2016 w			2039 s	2065 s	2079 m	2115 m-s
3a	2012 s	2020 s			2067 s	2081 m-s	2115 m
	2017 s			2041 m	2069 s	2083 m-s	2117 s
3b	2020 s	2027 s-m			2056/2067 m	2090 m,sh	2127 w,br
5a	2012 s,br		2031 vw		2058 s,br	2071 s,br	
				2041 s		2081 s	2117 s
5b	2020 s,br		2042 vw		2067 s	2081 s	
				2055 s		2093 s	2134 s

3. Solid-state NMR results and discussion

Multinuclear (^{13}C, ^{15}N, ^{207}Pb) magic-angle spinning magnetic resonance spectra have been obtained for the two anhydrous compounds $[(Me_3Pb)_4M(CN)_6]$, M = Ru (**5b**) and Fe (**5a**), and their hydrates. In the case of the Fe hydrate supposed to be **4a**, three separate samples were examined since it rapidly became clear from the ^{13}C spectra that mixtures of species were involved, including **5a** and at least one hydrate. We remain uncertain about the number of water molecules actually coordinated per formula unit in the latter. Indeed, as will be shown below, there is a discrepancy between the NMR in this case and single-crystal X-ray results. For **5a**/**b** and **4b**, however, all the available NMR information is consistent with asymmetric units comprising two EMe_3 groups and three cyanide units, as also found for **1a**/**b/c** [1] and by the present diffraction study of **4b** (Fig. 4).

The ^{15}N data are given in Table 6, together with information about related systems. In each case three signals of equal intensity (within experimental error) are seen. However, for the iron hydrate samples we believe the recorded resonances are actually those of the anhydrous compound since we would expect six signals for the hydrate (see the discussion on the methyl and cyanide ^{13}C signals). For the tin compounds the peak at lowest frequency was tentatively interpreted in terms of a substantial difference in chemical environment, possibly due to additional coordination of another Sn atom [1]. Such an explanation could still hold for the lead compounds, although the variations in shifts between the three signals are somewhat less marked in these cases, suggesting a more similar coordination geometry at all three sites. The ^{15}N spectra of **5a** and **5b** were obtained using an updated spectrometer and are of

Table 2
Selected ν(PbC) data of $[(Me_3Pb)_4M(CN)_6 \cdot nH_2O]$ systems from Raman spectra only

Sample	ν(PbC)/ cm^{-1} (Raman)	
2a	478 s	502 w-m
4a	476 s	500 w-m
4b	474 s	503 w-m
5a	472 s	504 sh; 497 m-w

Table 3
Summary of crystal data and details of data collection and refinement for **4a** (M = Fe) and **4b** (M = Ru)

Formula	$C_{18}H_{40}N_6O_2FePb_4$	$C_{18}H_{40}N_6O_2RuPb_4$
M_r (g mol^{-1})	1256.8	1302.4
Crystal size (mm)	$0.20 \times 0.25 \times 0.70$	$0.2 \times 0.3 \times 0.4$
Crystal system	Monoclinic	Monoclinic
Space group	$P2_1/c$	$P2_1/c$
a (Å)	10.208(2)	10.034(3)
b (Å)	13.588(3)	13.881(4)
c (Å)	12.094(3)	12.196(5)
β (°)	104.28(2)	100.95(3)
V(Å^3)	1625.7(6)	1667.8(1)
Z	2	2
$D_{calc.}$ (g cm^{-3})	2.567	2.593
F(000)	1119.90	1155.91
Temperature (K)	293	293
Diffractometer	Syntex Mod. $P2_1$	Syntex Mod. $P2_1$
Radiation λ (Å)	0.71073 (Mo–K_α)	0.71073 (Mo–K_α)
μ(Mo–K_α) (cm^{-1})	203.21	198.03
2θ range (°)	$4.5 < 2\theta < 50$	$4.5 < 2\theta < 50$
No. of reflections	3109	2642
No. of unique reflections	2823	2363
No. of reflections (refinement)	2490	2126
No. of refined parameters	145	149
Weighting scheme	$[\sigma^2(F) + 0.0001F^2]^{-1}$	$[\sigma^2(F) + 0.0001F^2]^{-1}$
Limit of significance	$[\|F_o\| > 6\sigma(F_o)]$	$[\|F_o\| > 6\sigma(F_o)]$
R, R_w	0.055, 0.055	0.049, 0.048
Absorption correction	Program DIFABS [8]	Program DIFABS [8]

Table 4
Selected interatomic distances (Å) for **4a** and **4b**

Distances	**4a** (Fe)	**4b** (Ru)
M–C(1)	1.88 (1)	2.00 (1)
M–C(2)	1.92 (2)	2.03 (1)
M–C(3)	1.89 (2)	2.03 (1)
C(1)–N(1)	1.21 (2)	1.19 (2)
C(2)–N(2)	1.11 (2)	1.15 (2)
C(3)–N(3)	1.16 (2)	1.15 (2)
N(1)–Pb(1)	2.51 (1)	2.55 (1)
N(2)–Pb(2)	2.35 (1)	2.32 (1)
N(3)–Pb(1)	2.56 (1)	2.54 (1)
Pb(2)–O(1)	2.66 (1)	2.68 (1)
Pb(1)–C(4)	2.21 (2)	2.18 (2)
Pb(1)–C(5)	2.20 (2)	2.20 (2)
Pb(1)–C(6)	2.20 (2)	2.18 (2)
Pb(2)–C(7)	2.22[a]	2.15 (3)
Pb(2)–C(8)	2.22[a]	2.22 (3)
Pb(2)–C(9)	2.22[a]	2.22 (3)
O(1)···N(1′)	2.94 (2)	2.85 (2)
O(1)···N(3′)	2.98 (2)	3.00 (2)

[a] Fixed value.

high-quality (Fig. 5), so that isotropic (^{207}Pb, ^{15}N) coupling data were derived (Table 6). In contrast to ^{15}N-enriched **1a** [1] the ^{15}N signals of **5a** and **5b** at highest frequency appear to lack the ^{207}Pb satellites.

Lead-207 and tin-119 information is also listed in Table 6, and the ^{207}Pb spectrum for the anhydrous ruthenium sample (**5b**) is shown in Fig. 6. Two bands are seen in each spectrum, though signals for the 'impurity' anhydrous component in the samples of **4a** are believed to obscure one resonance region of the dihydrate, itself. The two bands are of approximately equal intensity for pure **4b** and **5a**/**b**, though for the ruthenium hydrate they appear to be more in the ratio 1.5:1.0, probably because of varying cross-polarisation efficiency. Although the appearance of two signals for the lead compounds parallels the observations for the corresponding tin systems, the shift differences in the former are significantly smaller than for the latter, giving rise to speculation that the bonding may actually differ in some way. For **5a** and **5b** the high-frequency resonance is split into a 1:1:1 triplet (Fig. 6) which we believe arises from (^{207}Pb, ^{14}N) isotropic indirect coupling, the magnitude being comparable to that expected on the basis of the (^{207}Pb, ^{15}N) coupling effects in the ^{15}N spectra. This fact suggests either coordination of Pb to only one cyanide group, or substantial differences in ^{14}N relaxation times or in coupling constants for two different simultaneously bonded cyanide groups. The low-frequency ^{207}Pb resonances of **5a** and **5b** contains smaller, less well-resolved splittings involving an indeterminate number of components, showing that variations in relaxation and/or coupling do exist. Interestingly, for **4b** it is the low-frequency band which shows the clear 1:1:1 splitting, so that it is tempting to suggest a possible cross-over of bands on hydration. The ^{207}Pb spectrum for the iron hydrate shows a different (somewhat larger) splitting of the only clearly-visible band (around $\delta(^{207}\text{Pb})$ ca. 200 ppm). This we believe arises from crystallographic features which are reflected more clearly in the cyanide region of the ^{13}C spectrum (see below).

In all the ^{207}Pb spectra the spinning sideband manifolds cover a range of more than 2000 ppm, indicating substantial shielding anisotropy. Analysis of the intensity spread across the spinning sidebands suggests the anisotropies (defined as $\sigma_z - \sigma_{iso}$) are indeed ca. -1300 ppm and that shielding is approximately axially symmetric (as expected for trigonal bipyramidal systems with three equatorial methyl groups). Assignment of the ^{207}Pb chemical shifts presents a problem, since hydration apparently causes deshielding whereas in the corresponding Sn cases it leads to substantial shielding (Table 6). At least, owing to its triplet character, the signal of **4b** at 152 ppm is more likely to belong to the Pb(2) atom carrying one H_2O ligand.

As has been observed previously for cyanide-linked organometallic coordination polymers of the type $[(Me_3Sn)_4M(CN)_6 \cdot nL]$ $(n \geq 0)$, the cyanide region of the ^{13}C spectra for the three $(Me_3Pb)_4$-derivatives **4b** and **5a**/**b** reported herein consist of three resonances, each split into 2:1 doublets by second-order effects of dipolar coupling to quadrupolar ^{14}N nuclei (Fig. 7a). This shows, in conformity with the ^{15}N spectra, that the crystallographic asymmetric unit contains three cyanide groups. However, the pattern of signals is significantly different for the samples of the iron 'dihydrate', '**4a**' (Fig. 7b). It has proved possible to distinguish resonances from the anhydrous form **5a**, present at a high level as an 'impurity'. The additional signals, assignable to a hydrate show not only the three bands expected, each with a 2:1 splitting, but also a doubling of each peak, with modest splittings (ca. 1 ppm) and equal

Table 5
Selected bond angles (°) in the structures of **4a** and **4b**

Angles	**4a** (Fe)	**4b** (Ru)
C(1)–N(1)–Pb(1)	120.1 (1.0)	121.1 (1.0)
C(2)–N(2)–Pb(2)	178.9 (1.3)	177.1 (1.5)
C(3)–N(3)–Pb(1)	126.0 (1.0)	124.0 (1.5)
N(1)–Pb(1)–N(3)	171.4 (0.4)	173.1 (0.5)
N(2)–Pb(2)–O(1)	175.0 (0.5)	175.4 (0.6)
C(4)–Pb(1)–N(1)	87.2 (0.6)	87.3 (0.6)
C(5)–Pb(1)–N(1)	89.1 (0.6)	87.9 (0.7)
C(6)–Pb(1)–N(1)	91.6 (0.6)	92.4 (0.6)
C(7)–Pb(2)–N(2)	99.4 (1.5)	95.9 (0.9)
C(8)–Pb(2)–N(2)	92.8 (1.6)	94.6 (0.7)
C(9)–Pb(2)–N(2)	87.3 (1.5)	92.6 (0.8)
C(7)–Pb(2)–O(1)	84.4 (1.5)	81.9 (0.9)
C(8)–Pb(2)–O(1)	82.7 (1.6)	94.6 (0.7)
C(9)–Pb(2)–O(1)	92.3 (1.5)	85.7 (0.8)

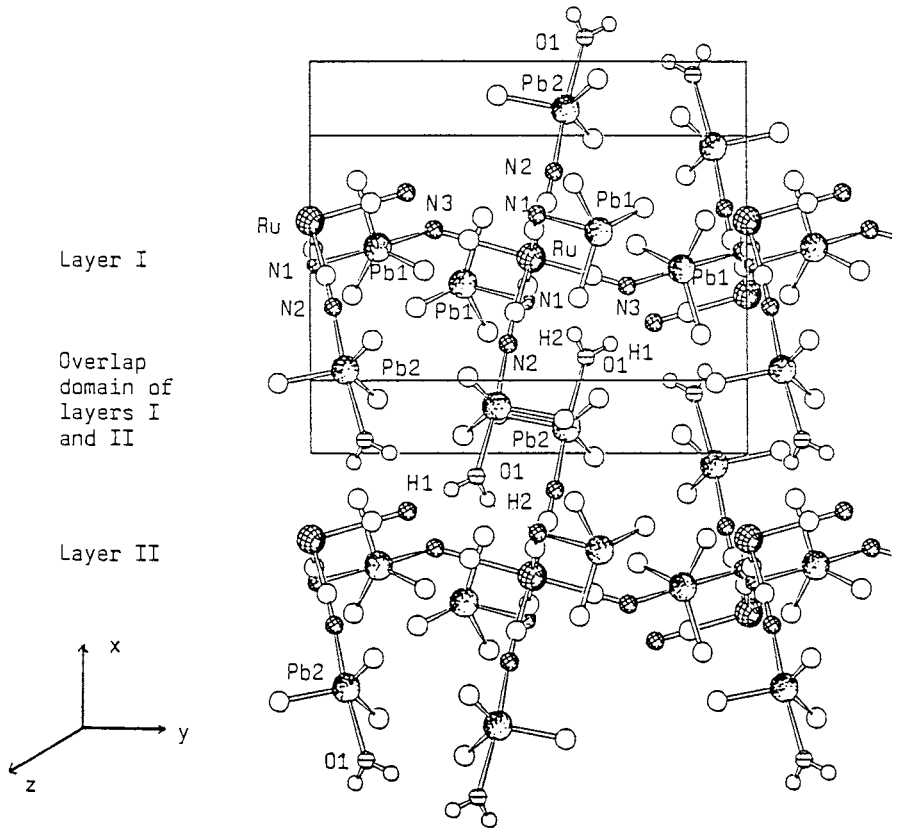

Fig. 3. Crystal structure with partial atomic numbering scheme (see also Fig. 4) of **4b** (SCHAKAL plot). The layers I, II, etc. contain only the lead atoms Pb(1) of one layer, while the 'overlap domain' contains exclusively Pb(2) atoms of two adjacent layers.

intensities (Fig. 7b). This strongly suggests a doubling of the number of atoms in the asymmetric unit of '**4a**' (compared to that of **4b**) but with environments which are very similar. Such a conclusion is consistent with the ^{207}Pb and ^{13}C (methyl) spectra (Fig. 8). It is possible that the hydrate on which the NMR results were obtained differs from that (true **4a**) which was used for the single-crystal diffraction study in the number of water molecules per lead atom. Another explanation could be that the disorder of the Me_3Pb fragments of chain B in **4a** (vide supra) might cause alternative environments (but not distinguishable atomic coordinates!) and, hence, weak splittings of the corresponding NMR signals.

The true chemical shifts (at the weighted average of the 2:1 doublets) and the splittings for **4a**/**b** and **5a**/**b**, plus various tin analogues, are reported in Table 7. The pattern of shifts is very similar for the corresponding Ru and Fe compounds, but they span a much wider range for the lead systems (ca. 18 ppm) than for the tin compounds (ca. 8 ppm). The effect of hydration on the shifts for the lead compounds is minimal for the outermost resonances, but marked (ca. 7 ppm deshielding) for the intermediate signals. Table 6 shows that there is a similar effect on the ^{15}N shifts for the ruthenium compounds—again it is only the resonance at intermediate frequency that is substantially changed (9 ppm deshielding) by hydration. Two facts emerge, (i) the intermediate frequencies in the ^{13}C and ^{15}N spectra should correspond to the same cyanide group (and we anticipate an analogous correspondence for the outer bands); and (ii) only this particular cyanide group experiences a significant change in environment on hydration. Logic suggests that the cyanide group whose resonances are most affected is the one trans to a water oxygen atom in the hydrates. Interestingly, only one of the three Raman-active ν(CN) bands turns out to be significantly displaced when the spectra of **4a**/**b** are compared with those of **5a**/**b** (vide supra). On the other hand, the X-ray data for the two lead dihydrates indicate that the two non-equivalent cyanide groups in chain A are substantially bent at nitrogen (Pb–N–C angles 120–126°) and might therefore be reasonably well-prepared for hydrogen bonding to the water molecules of chain B. Hence, chain A should also show pronounced cyanide ^{13}C and ^{15}N chemical shift changes when dehydration occurs. While apparently the presence of hydrogen bonds in **4a**/**b** is not impressively supported by any of the solid-state NMR results, a comparison of the cyanide ^{13}C- and ^{15}N data of **1a** with those of **7** (Tables 6 and 7) strongly suggests that just one cyanide group of **1a** is affected probably owing to

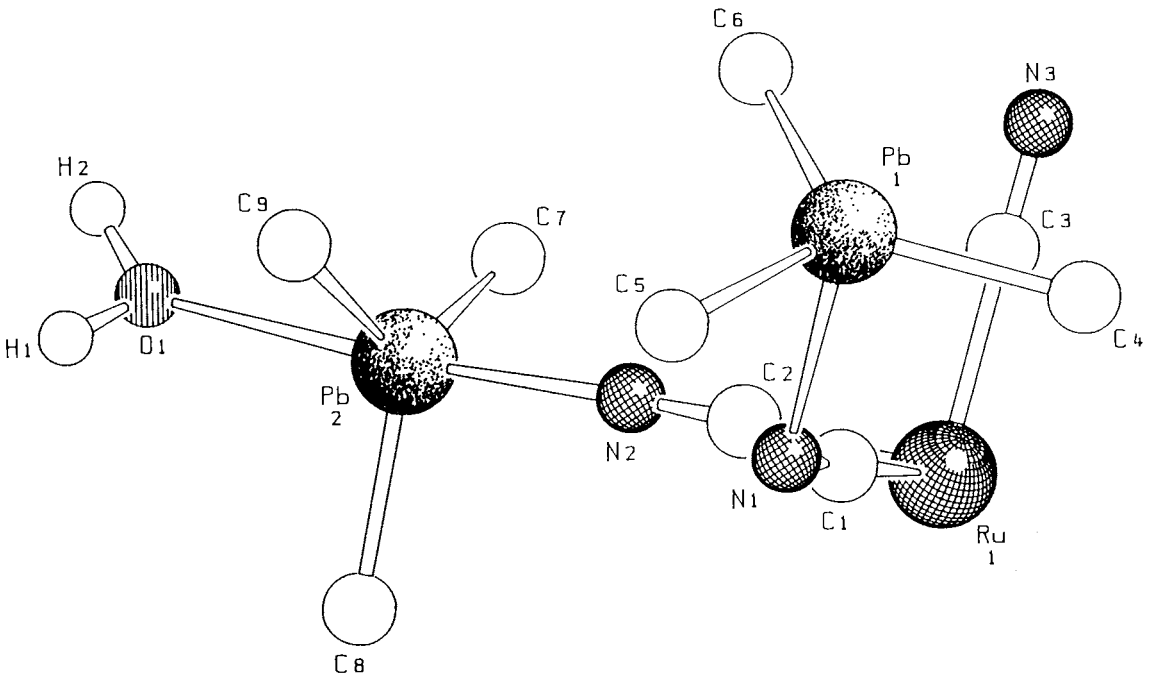

Fig. 4. Asymmetric unit of **4b** (SCHAKAL plot).

its interaction with two Me_3Sn units, while in **7** all six CN ligands carry only one Me_3Sn group [1,9]. Another feature worthy of comment is the remarkable sharpness of the components of the 2:1 doublets (each component ca. 30–40 Hz in width), which contrasts with the situation for the tin systems. We have no current explanation for this, given that each component is in principle a powder pattern, but note that the bandshapes of the spinning sidebands differ from those of the centrebands [21].

The methyl regions of the ^{13}C spectra for both anhydrous lead compounds (**5a**/**b**) are temperature dependent. At low temperatures ($< 20°C$ for **5a** and $< -20°C$ for **5b**) six major signals are obtained, spread over ca. 8 ppm. The relevant data are given in Table 8, and a detailed investigation of the exchange kinetics is under way. At ambient probe temperature approximately two broad lines are observed. Undoubtedly the phenomenon giving rise to these observations is the partially hindered internal rotation of Me_3Pb groups, such as we have reported for the corresponding tin compounds [13,14]. However, in the case of the hydrated species, decreasing the temperature only has a marginal effect on linewidths, and no further splittings are seen in the temperature range -60 to $+40°C$. For the ruthenium dihydrate, **4b**, two widely-separated methyl carbon signals, of approximately equal intensity, are observed (Fig. 8a), the one at higher frequency being notably broad. The CH_3 region of '**4a**' is again complicated by the signals of the anhydrous derivative, but one sharp doublet (with ^{207}Pb satellites) is clearly visible at low frequency (Fig. 8b). and we suspect the presence of a broad signal at higher frequency, as in the ruthenium case. The doublet character of the low-frequency resonance is presumably again a consequence of the crystallographic effects discussed above. One reason for the apparently much slower Me_3Pb-rotation in **5a**/**b** (than in the corresponding hydrates),which is responsible for the strong temperature dependence of the spectra of **5a**/**b**, is the presumably even tighter crystal packing of the two anhydrous species, which is also suggested by the corresponding formula volumes (vide supra).

4. Conclusions

From the foregoing discussion it has become evident that the presence or absence of water molecules (at most two per formula unit) is of crucial importance for the supramolecular architecture, as well as for the presence of occasional 'impurities' in, and the resulting spectroscopic (IR/Ra, CP MAS NMR) properties of the final lead-containing samples. Moreover, the specific affinity of a Me_3E^+ fragment (E = Sn or Pb) towards H_2O must be appropriately balanced in view of the presence or absence of ion-exchange activity. The potential ability of N atoms incorporated into $-M-C{\equiv}N \rightarrow E \leftarrow N{\equiv}C-M-$ chains to take part in hydrogen bonding with H_2O molecules could, in principle, promote either a cleavage of $N \rightarrow E$ bonds (then facilitating eventual ion-exchange), or might interlink adjacent building blocks like the layers of the primary structure of the diaqua title compounds **4a** and **4b**. Unfortu-

Table 6
^{15}N and metal (^{207}Pb or ^{119}Sn) NMR data of several $[(Me_3E)_4M(CN)_6 \cdot nH_2O]$ systems

Sample	E	M	n	δ_N (ppm)			$\lvert J_{EN}\rvert$ (Hz)[a]			δ_E (ppm)		$\lvert JEN\rvert$/Hz[b]
5b	Pb	Ru	0	−128	−141	−154	[c]	264	315	130[d]	75	ca. 220
5a	Pb	Fe	0	−119	−132	−146	[c]	267	315	139[d]	71	ca. 200
4b	Pb	Ru	2	−127	−132	−159	[c]	[c]	345	201	152[d]	ca. 240
'4a'	Pb	Fe	x	−120[e]	−133[e]	−147[e]	[c]:	[c]	[c]	200/190	ca. 140[f]	[c]
1b [1]	Sn	Ru	0	−118	−136	−166	[c]	[c]	[c]	32	−97	[c]
1a [1]	Sn	Fe	0	−109	−124	−161	120	167	[c]	46	−108	[c]
7 [1,12][g]	Sn	Fe	2	−116[h]	−125		[c]	[c]	[c]	−73	−136	[c]

[a] Derived from ^{15}N spectra and listed in the same order as the chemical shifts.
[b] Derived from ^{207}Pb spectra and therefore relating to ^{207}Pb, ^{14}N coupling.
[c] Not obtained.
[d] Clean triplet.
[e] The state of purity of this sample (see the text) and the poor S/N in the spectrum leaves us uncertain whether these values are those of the hydrate or of the anhydrous form but we believe they are probably of the latter.
[f] Believed to be obscured by bands from the anhydrous compound.
[g] Also with one molecule of dioxane per Fe atom.
[h] About twice as intense as the resonance at −125 ppm.

nately, even results of the otherwise most informative techniques such as X-ray crystallography and multinuclear solid-state magnetic resonance have turned out not to be entirely satisfactory for a firm proof of the suspected tricoordination of the nitrogen atoms N(1) and/or N(3) in the lattice of **4a**/**4b**. Tricoordinated N atoms may also be postulated to interpret the experimental evidence of exclusively t.b.p.-configured Me_3E units in the anhydrous compounds **1a**/**b**/**c** and **5a**/**b**. Structural alternatives would consist of the presence of two *trans*-oriented (per M atom) isocyanide ligands, $CNEMe_3$, with tetracoordinated E. Although a few organometallic complexes involving such ligands have already been described [15], all our earlier [1] and present spectroscopic results appear not to be in favour of such terminal $-M-CN-EMe_3$ units which would, moreover, be expected to display chemically quite labile metal to (isocyanide) carbon bonds. Future tasks to overcome the still-pending problems will inter alia include further attempts to arrive at a single crystal of **5a** or **5b** (as well as of **1a**-**1c**), and to subject, for better comparison, complexes with genuine stanna-and plumba-isocyanide ligands to detailed IR/Ra- and multinuclear magnetic resonance studies.

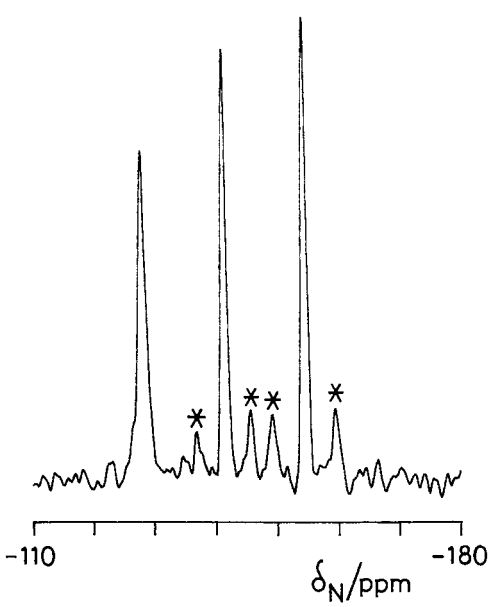

Fig. 5. Nitrogen-15 CP MAS spectrum at 30.40 MHz of $[(Me_3Pb)_4Ru(CN)_6]$, **5b** (natural abundance of ^{15}N and centreband region only), showing the satellite signals (indicated by asterisks) arising from coupling to ^{207}Pb for two of the centrebands. In contrast to the other spectra illustrated in this paper, this one was recorded after upgrading the Varian spectrometer with a Unity Plus console. Spectrometer operating conditions: contact time, 9 ms; recycle delay, 1 s; 49500 transients; spin rate 4570 Hz.

5. Experimental details

All $[(Me_3Pb)_4M(CN)_6 \cdot nH_2O]$ systems (M = Fe or Ru) with $n < 2.0$ were obtained from concentrated aqueous solutions of Me_3PbCl and $K_4[M(CN)_6 \cdot 3H_2O$. In a typical synthesis, a clear solution of 0.5 g (1.8 mmol) of Me_3PbCl in 50 ml of H_2O was added (without stirring) to a solution of 0.17 g (0.45 mmol) of $K_4[Fe(CN)_6] \cdot 3H_2O$ in 40 ml of H_2O. After filtration and washing with a little cold H_2O, the white precipitate was dried in vacuo either at room temperature or at 60–80°C for 2 days, affording **2a** and **5a**, respectively (yield of **5a**: 0.46 g or 84%). Drying at 60–80°C and ambient pressure led to **3a**, while **4a** crystallized within 2 days from an initially clear solution of Me_3PbCl and $K_4[Fe(CN)_6] \cdot 3H_2O$ in about 150 ml of H_2O. After filtration, this preparation was dried at room temperature and ambient pressure.

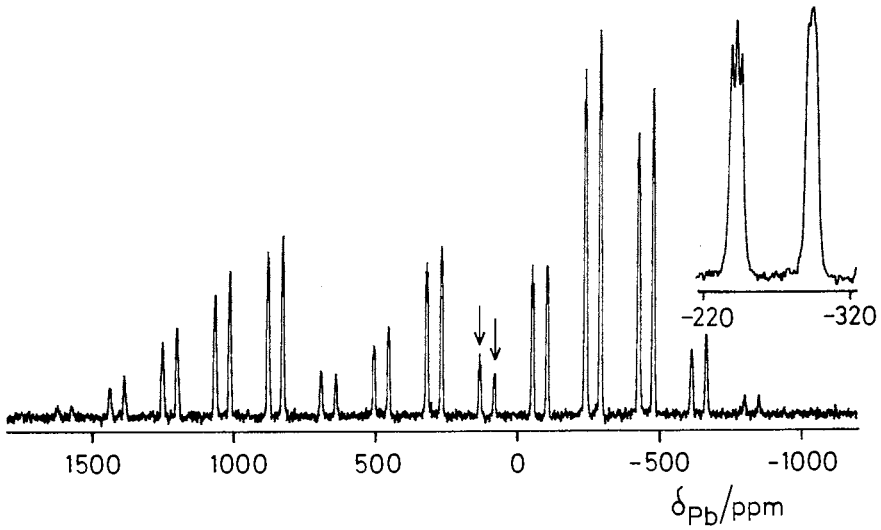

Fig. 6. Lead-207 CP MAS spectrum at 62.74 MHz of $[(Me_3Pb)_4Ru(CN)_6]$, **5b**. The arrows indicate the centrebands. The inset shows an expansion of the second-order low-frequency spinning sidebands to show the coupling to ^{14}N. Spectrometer operating conditions: contact time, 7.5 ms; recycle delay, 1 s; 48500 transients; spin rate 11650 Hz.

Analysis found for **2a**: C, 17.35; H, 2.70; N, 6.77; O, 1.20. $C_{18}H_{38}N_6OFePb_4$ calculated: C, 17.45; H, 3.09; N, 6.78; O, 1.29%. Analysis found for **4a**: C, 17.28; H, 3.29; N, 6.69. $C_{18}H_{40}N_6O_2FePb_4$ calculated: C, 17.20; H, 3.21; N, 6.68%. Analysis found for **5a**: C, 17.66; H, 2.85; N, 6.84; Fe, 4.49; Pb, 67.81. $C_{18}H_{36}N_6FePb_4$ cal-

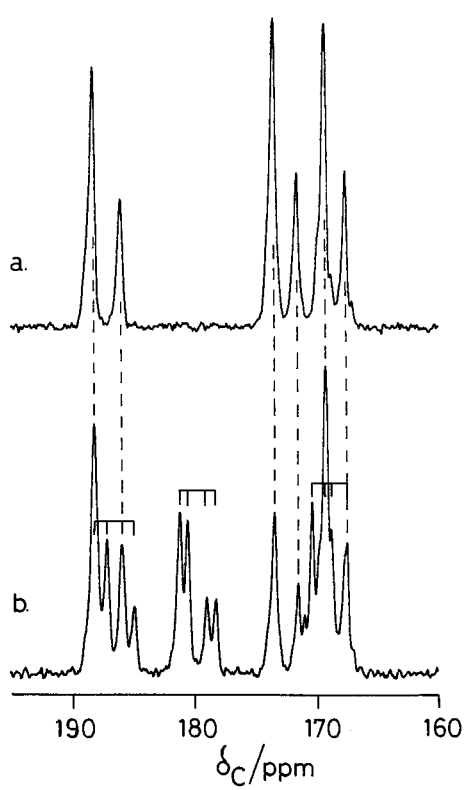

Fig. 7. Cyanide region of the 75.43 MHz ^{13}C CP MAS spectra at ambient probe temperature of (a) $[(Me_3Pb)_4Ru(CN)_6 \cdot 2H_2O]$, and (b) $[(Me_3Pb)_4Fe(CN)_6 \cdot nH_2O]$. The signal groupings mentioned in the text are indicated. Spectrometer operating conditions: relaxation delay, 1 s; contact time, 9 ms; spin rate, 4850 Hz (a) and 4620 Hz (b); number of transients, 56100 (a) and 51700(b).

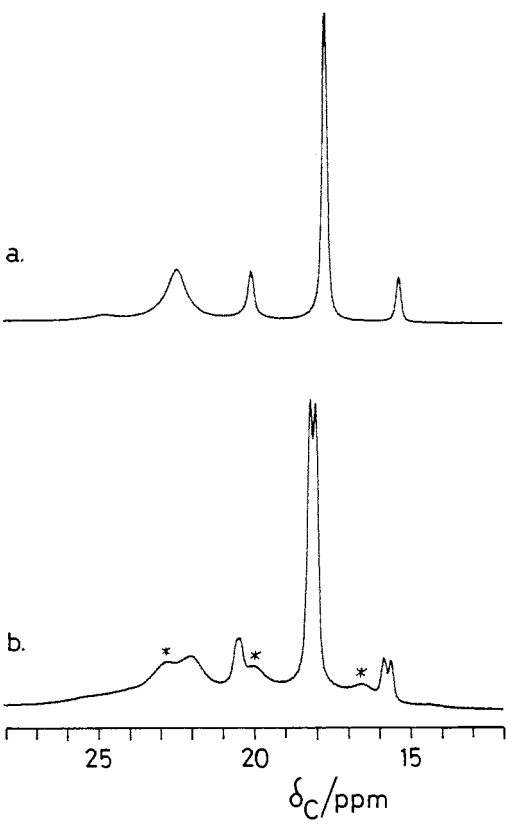

Fig. 8. Methyl region of the 75.43 MHz ^{13}C CP MAS spectra at ambient temperature of (a) $[(Me_3Pb)_4Ru(CN)_6 \cdot 2H_2O]$, **4b**, and (b) $[(Me_3Pb)_4Fe(CN)_6 \cdot nH_2O]$, **4a**. For (b), peaks which probably arise from the anhydrous form **5a** are indicated by asterisks. Spectrometer operating conditions are identical to those given in Fig. 7.

Table 7
Cyanide ^{13}C chemical shifts and second-order splittings (with ^{14}N) of several $[(Me_3E)_4M(CN)_6 \cdot nH_2O]$ systems

Sample	E	M	*n*	δ_C(CN) (ppm)			Splitting (Hz)[a]		
5b	Pb	Ru	0	174.3	160.2	155.4	180	149	128
5a	Pb	Fe	0	187.3	172.7	168.6	176	146	127
4b	Pb	Ru	2	173.6	167.4	155.5	178	170	122
'**4a**'	Pb	Fe	x	187.4	180.3	169.8	172	165	118
				186.3	179.7	168.6	168	174	137
1b [1]	Sn	Ru	0	ca. 166	163.1	158.8	[b]	90	133
1a [1]	Sn	Fe	0	178.4	174.8	169.2	85	153	130
7 [1][c]	Sn	Fe	2	177.1	172.7	167.5	116	151	137

[a] Arising from residual (^{14}N, ^{13}C) dipolar coupling. Listed in the same order as the chemical shifts.
[b] Not obtained.
[c] Also with one molecule of dioxane per Fe atom.

culated: C, 17.70; H, 2.97; N, 6.88; Fe, 4.57; Pb, 67.87%. Analysis found for **4b**: C, 16.62; H, 3.14; N, 6.48; Ru, 7.59; Pb, 63.68. $C_{18}H_{40}N_6O_2RuPb_4$ calculated: C, 16.60; H, 3.10; N, 6.45; Ru, 7.76; Pb, 63.63%. Analysis found for **5b**: C, 17.06; H, 3.02; N, 6.59. $C_{18}H_{36}N_6RuPb_4$ calculated: C, 17.07; H, 2.87; N, 6.64%.

Infrared spectroscopic measurements were carried out on a Perkin-Elmer (PE) FT-IR-1720 instrument (studying both KBr pellets and Nujol mulls). Raman spectra were run on a Ramanov U-1000 spectrometer of Jobin Yvon (studying polycrystalline particles in a glass capillary). Well-shaped crystals of **4a** and **4b** were selected for X-ray crystallography before the crystal surfaces had become absolutely dry. Crystal data of relevance are given in Table 3 [16]. The structures were solved and refined using Patterson methods [17,18]. All nonhydrogen atoms, including the disordered Me_3Pb groups of **4a** were anisotropically refined. Hydrogen atoms are not included in the calculation, and three Pb–C distances of **4a** were fixed to 2.22 Å (Table 4). Atomic positions of **4a** and **4b** are listed in Table 9 and Table 10.

Only materials supposed to be, according to their vibrational spectra, pure **4a**, **4b**, **5a** and **5b**, respectively, were selected for solid-state NMR spectroscopic studies. All ^{13}C and ^{207}Pb spectra. together with the ^{15}N spectra of the hydrates, were recorded on a Varian VXR-300 spectrometer using Doty MAS probes with cross-polarisation and high-power proton decoupling. The ^{15}N spectra of the anhydrous samples were obtained after the spectrometer was upgraded to a Unity Plus system. For ^{13}C and ^{15}N at 75.43 MHz and 30.40 MHz, respectively, 7 mm o.d. rotors were used at spin-rates of 4–5 kHz, whereas for ^{207}Pb at 62.74 MHz. 5 mm o.d. rotors were used at spin-rates of 11.5–13.5 kHz. All spectra were recorded with a 1 s relaxation delay, contact times of between 5 and 10 ms and 30000–70000 repetitions (in the case of ^{13}C this was in order to observe the CN signals). Chemical shifts, obtained by sample replacement, are quoted using the high-frequency-positive convention, in ppm with respect to $SiMe_4$ for ^{13}C, NH_4NO_3 for ^{15}N (nitrate line) and $PbMe_4$ for ^{207}Pb. Analyses of ^{207}Pb sideband manifolds were carried out using a sideband fitting program [19] based on the theory described by Maricq and Waugh [20].

Table 8
Methyl ^{13}C chemical shifts and coupling constants for several $[(Me_3E)_4M(CN)_6 \cdot nH_2O]$ systems

Sample	E	M	*n*	δ_C(ave) (ppm)	$\lvert J_{EC}\rvert$ (ave) (Hz)[a]	$^{\delta}$C(low T) (ppm)	$\lvert J_{EC}\rvert$ (low T) (Hz)[a]
5b	Pb	Ru	0	19.4, 18.8	[b]	24.0, 21.9, 18.9, 18.3, 16.0, 15.7	470, [b], [b], [b], 312, 352
5a	Pb	Fe	0	20.1, 19.5	[b]	24.7, 22.7, 19.7, 18.9, 16.6, 16.1	480, [b], [b], [b], 304, 334
4b	Pb	Ru	2	22.4[c], 17.7	349, 356	[b]	[b]
'**4a**'	Pb	Fe	x	18.0[d]	362	[b]	[b]
				18.1	354		
1b [14]	Sn	Ru	0	4.3, 1.4	470, 440	9.2, 4.4, 2.8, 2.4, 1.4, −2.1	581, 429, 536, 439, 457, 405
1a [14]	Sn	Fe	0	4.3, 1.2	550, 430	8.9, 3.8, 2.8, 1.7, 1.3, −2.5	577, 464, 557, 430, 477. 415
7 [12][b]	Sn	Fe	2	2.3, 0.9	562, 528	[b]	[b]

[a] Listed in the order of the chemical shifts.
[b] Not obtained.
[c] Broad.
[d] Also a broad signal in the region δ_C 22 ppm.
[e] Also with one molecule of dioxane per Fe atom.

Table 9
Atomic coordinates for **4a**. The positions of C(7′)–C(9′) correspond to disordered $Me_3Pb(2)$ units

Atom	x/a	y/b	z/c	U_{eq}
Pb(1)	0.49454(6)	0.65555(4)	0.86144(5)	0.0299(2)
Pb(2)	−0.00596(7)	0.60474(6)	0.28288(5)	0.0452(3)
Fe(1)	0.50000	0.50000	0.50000	0.0452(3)
N(1)	0.4245(15)	0.5106(9)	0.7314(11)	0.040(5)
N(2)	0.2165(15)	0.5618(11)	0.3757(11)	0.050(5)
N(3)	0.5842(15)	0.7158(8)	0.5157(11)	0.037(4)
C(1)	0.4548(16)	0.5070(10)	0.6413(11)	0.029(4)
C(2)	0.3211(16)	0.5409(11)	0.4211(12)	0.031(5)
C(3)	0.5566(15)	0.6330(12)	0.5111(12)	0.032(5)
C(4)	0.7060(18)	0.6173(15)	0.8640(16)	0.056(7)
C(5)	0.3756(18)	0.5954(13)	0.9752(14)	0.045(6)
C(6)	0.3874(22)	0.7581(13)	0.7289(15)	0.060(7)
C(7)	0.0265(57)	0.6523(28)	0.1162(20)	0.089(16)
C(8)	−0.0779(59)	0.4504(15)	0.2810(47)	0.108(19)
C(9)	−0.0180(57)	0.6802(26)	0.4428(21)	0.090(17)
C(7′)	0.0053(66)	0.5678(42)	0.1067(22)	0.121(22)
C(8′)	−0.0934(70)	0.5328(41)	0.4131(37)	0.139(27)
C(9′)	0.0213(40)	0.7668(4)	0.2959(31)	0.057(10)
O(1)	−0.2650(13)	0.6396(11)	0.1857(12)	0.067(9)
H(1)	−0.3530(177)	0 6008(245)	0.1804(290)	0.246(142)
H(2)	−0.2912(306)	0.6866(188)	0.1177(271)	0.246(142)

Table 10
Atomic coordinates for **4b**

Atom	x/a	y/b	z/c	U_{eq}
Pb(1)	0.49657(7)	0.34575(4)	0.13168(5)	0.0226(2)
Pb(2)	−0.01719(7)	0.57967(5)	0.27733(6)	0.0330(2)
Ru(1)	0.50000	0.50000	0.50000	0.0139(5)
N(1)	0.580(1)	0.487(1)	0.260(1)	0.031(5)
N(2)	0.202(1)	0.553(1)	0.375(1)	0.043(6)
N(3)	0.408(1)	0.220(1)	−0.015(1)	0.028(5)
C(1)	0.553(1)	0.493(1)	0.350(1)	0.024(5)
C(2)	0.310(1)	0.537(1)	0.420(1)	0.021(5)
C(3)	0.442(1)	0.140(1)	−0.010(1)	0.019(5)
C(4)	0.291(2)	0.391(1)	0.140(1)	0.040(6)
C(5)	0.620(2)	0.402(1)	0.015(3)	0.059(9)
C(6)	0.598(3)	0.241(1)	0.252(1)	0.061(8)
C(7)	0.042(3)	0.643(2)	0.133(2)	0.09(1)
C(3)	−0.066 (2)	0.424(1)	0.252(2)	0.0756(9)
C(9)	−0.078(3)	0.655(2)	0.421(2)	0.09(1)
O(1)	−0.066(2)	0.625(1)	0.165(1)	0.071(6)
H(1)	−0.33(1)	0.60(1)	0.22(1)	0.08(6)
H(2)	−0.31(3)	0.683(9)	0.12(1)	0.08(6)

Acknowledgements

We thank the UK Science and Engineering Research Council for access to the Varian VXR 300 spectrometer under the national solid-state NMR service arrangements. Financial support from the British Council and the DAAD (Bonn) under the ARC Programme, from Deutsche Forschungsgemeinschaft (until 1992) and from the Fonds der Chemischen Industrie is greatly appreciated. Professor U. Behrens, Dr S. Eller, Dr D.C. Apperley, K. Rechter and (the late) T.M. Soliman are thanked for helpful discussions (U.B., D.C.A.) and the delivery of single samples or spectra (S.E., K.R., T.M.S.), respectively.

References

[1] S. Eller, P. Schwarz, A.K. Brimah, R.D. Fischer, D.C. Apperley, N.A. Davies, R.K. Harris, Organometallics 12 (1993) 3232.
[2] S. Eller, P. Brandt, A.K. Brimah, P. Schwarz, R.D. Fischer, Angew Chem. 101 (1989) 1274. (b) S. Eller, P. Brandt, A.K. Brimah, P. Schwarz, R.D. Fischer, Angew Chem. Int. Ed. Engl. 28 (1989) 1263.
[3] S. Eller, M. Adam, R.D. Fischer, Angew Chem. 102 (1990) 1157. (b) S. Eller, M. Adam, R.D. Fischer, Angew Chem. Int. Ed. Engl. 29 (1990) 1126.
[4] P. Schwarz, Doctoral Dissertation, University of Hamburg, Germany, 1994.
[5] Thus in dioxane, ion-exchange according to Eq. 1 was not observed until a few drops of water had been added: Ref. 4, pp. 15.
[6] U. Behrens, A.K. Brimah, T.M. Soliman, R.D. Fischer, D.C. Apperley, N.A. Davies, R.K. Harris, Organometallics 11 (1992) 1718.
[7] U. Nolte, R.D. Fischer, unpublished results.
[8] A.K. Brimah, Doctoral Dissertation, University of Hamburg, Germany, 1991.
[9] M. Adam, A.K. Brimah, R.D. Fischer, X.F. Li, Inorg. Chem. 29 (1990) 1595.
[10] U. Behrens, A.K. Brimah, R.D. Fischer, J. Organomet. Chem. 411 (1991) 325.
[11] G.M. Sheldrick, R. Taylor, Acta Crystallogr. Section B 31 (1975) 2740.
[12] D.C. Apperley, N.A. Davies, R.K. Harris, A.K. Brimah, S. Eller, R.D. Fischer, Organometallics 9 (1990) 2672.
[13] D.C. Apperley, N.A. Davies, R.K. Harris, S. Eller, P. Schwarz, R.D. Fischer, J. Chem. Soc. Chem. Comm. (1992) 740.
[14] R.K. Harris, M.M. Sünnetçioglu, R.D. Fischer, Spectrochim. Acta Ser. A 50 (1994) 2069.
[15] H. Behrens, M. Moll, W. Popp, J.H. Seibold, E. Sepp, P. Würstl, J. Organomet. Chem. 192 (1980) 389.
[16] Further details about the X-ray structures may be obtained from the Fachinformationszentrum, Karlsruhe, Gesellschaft Für wissenschaftlich technische Intormation m.b.H., D-76344 Eggenstein-Leopoldshafen (Germany) on quoting the depository number CSD-58692, the names of the authors, and the journal citation.
[17] G.M. Sheldrick, SHELX-76, Programs for Crystal Structure Determination, University of Cambridge, England, 1976.
[18] G.M. Sheldrick, SHELXS-86, Programs for Crystal Structure Solution, Universität Göttingen, Germany, 1986.
[19] L.H. Merwin, H. Bai, Sideband fitting program, University of Durham (1987, 1991).
[20] M.M. Maricq, J.S. Waugh, J. Chem. Phys. 70 (1979) 3300.
[21] N.A. Davies, R.K. Harris, A.C. Olivieri, Mol. Phys. 87 (1996) 669.